PNAS
www.pnas.org

Supplementary Information for

Lightweight, flaw-tolerant and ultrastrong nanoarchitected carbon

Xuan Zhang, Andrey Vyatskikh, Huajian Gao, Julia R. Greer, Xiaoyan Li

Corresponding authors: Huajian Gao, Julia R. Greer, and Xiaoyan Li
Email: Huajian_Gao@brown.edu (H.G.), jrgreer@caltech.edu (J.G.), and xiaoyanlithu@tsinghua.edu.cn (X.L.)

This PDF file includes:

Figs. S1 to S7
Table S1
Captions for movies S1 to S2

Other supplementary materials for this manuscript include the following:

Movies S1 to S2

www.pnas.org/cgi/doi/10.1073/pnas.1817309116

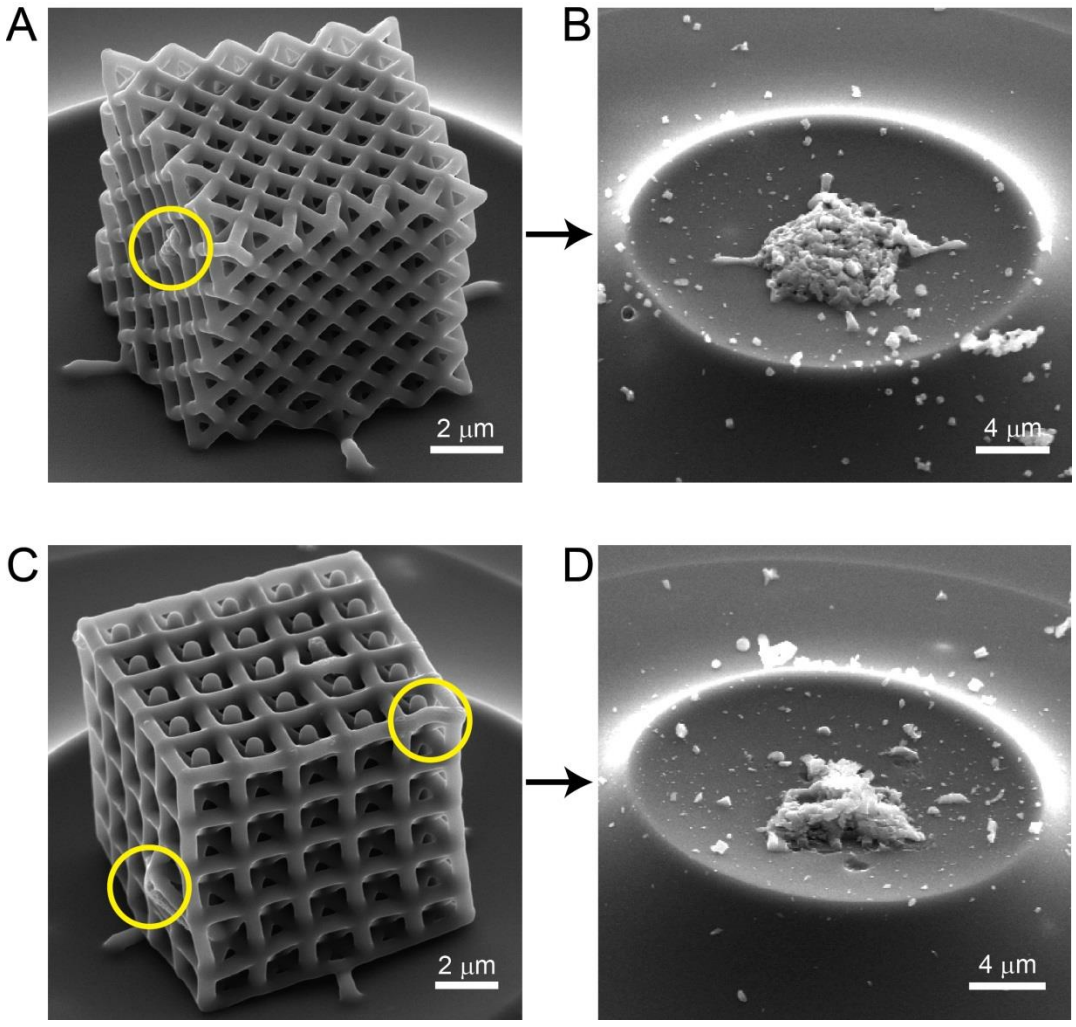

Fig. S1. SEM images of typical octet- and iso-truss nanolattices before and after compression. (*A*, *B*) SEM images of an octet-truss nanolattice with d=382 nm. (*C*, *D*) SEM images of the iso-truss nanolattice with d_1=538 nm and d_2=612 nm. The images in (*B*) and (*D*) indicate brittle failure of nanolattices.

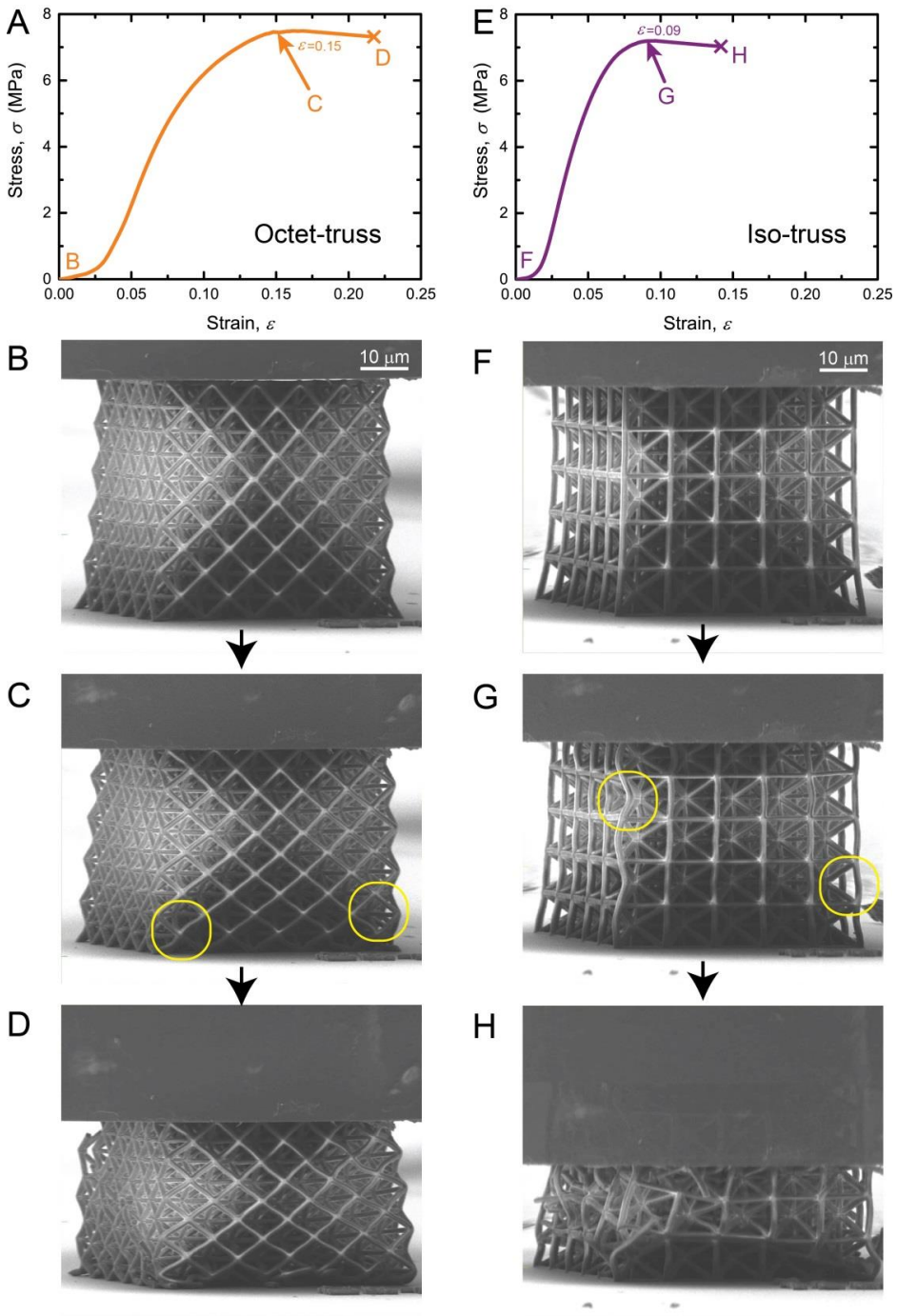

Fig. S2. In-situ compression tests on polymer nanolattices. (*A*) Compressive stress-strain curve of octet-truss nanolattice with d=1.12 μm. (*B-D*) SEM snapshots of deformed octet-truss nanolattice under different compressive strains. (*E*) Compressive stress-strain curve of iso-truss nanolattice with d_1=1.30 μm and d_2=1.49 μm. (*F-H*) SEM snapshots of deformed iso-truss nanolattice under different compressive strains. The circled regions in (*C*) and (*G*) indicate the buckling of struts during compression.

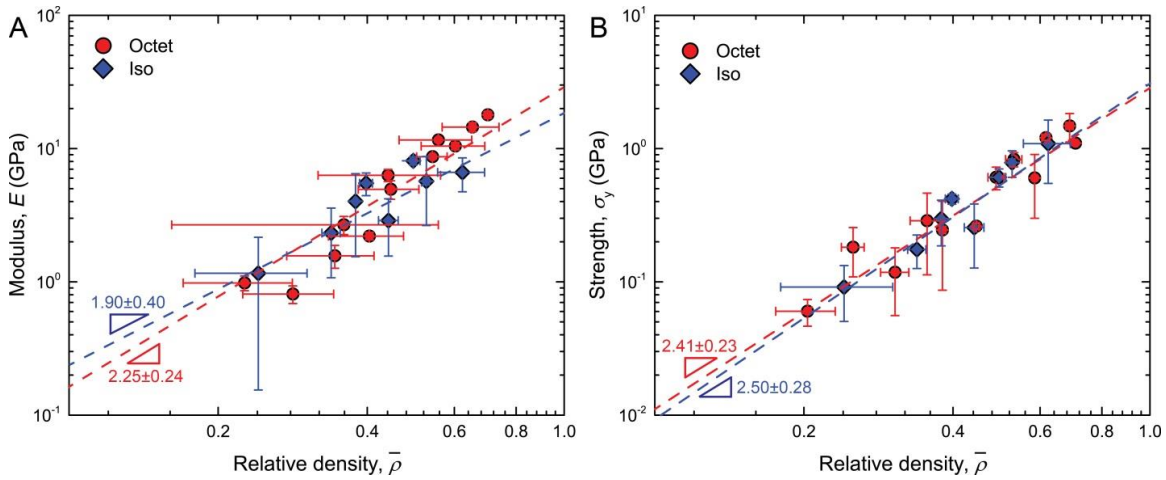

Fig. S3. Young's modulus and compressive strength versus density of pyrolytic carbon nanolattices. (*A*,*B*) Young's modulus and strength versus relative density of octet- and iso-truss pyrolytic carbon nanolattices on log-log scale. Scaling power law slopes are indicated for each architecture. Error bars represent the standard deviations from the average over some data of samples with comparable densities.

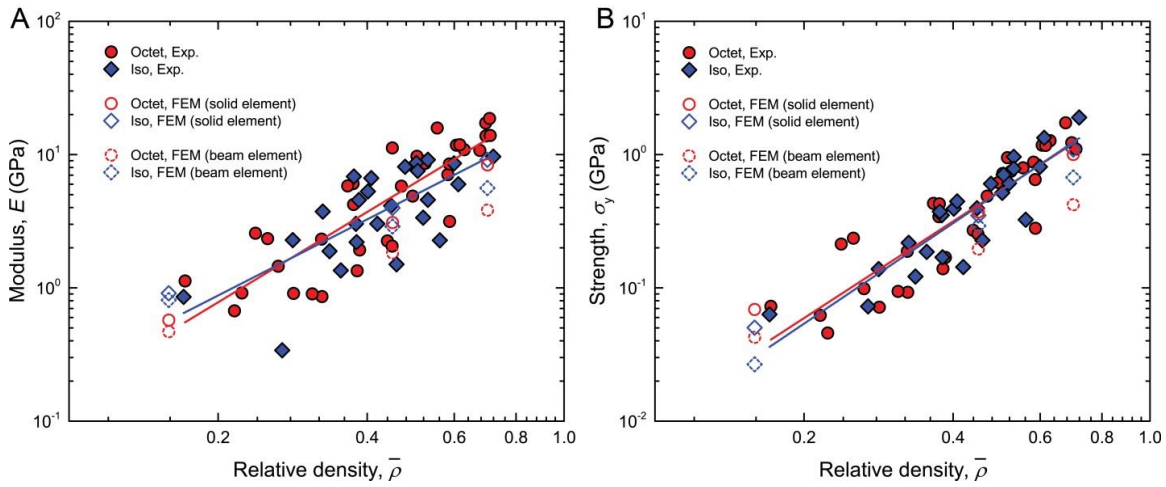

Fig. S4. Comparison between finite element modelling and experimental results. (*A*, *B*) Modulus versus relative density and strength versus relative density from finite-element modelling and experiment. While the modelling results based on solid elements are in good agreement with those from experimental measurements, those based on beam elements exhibit similar trend but larger deviations from experiments at higher relative densities.

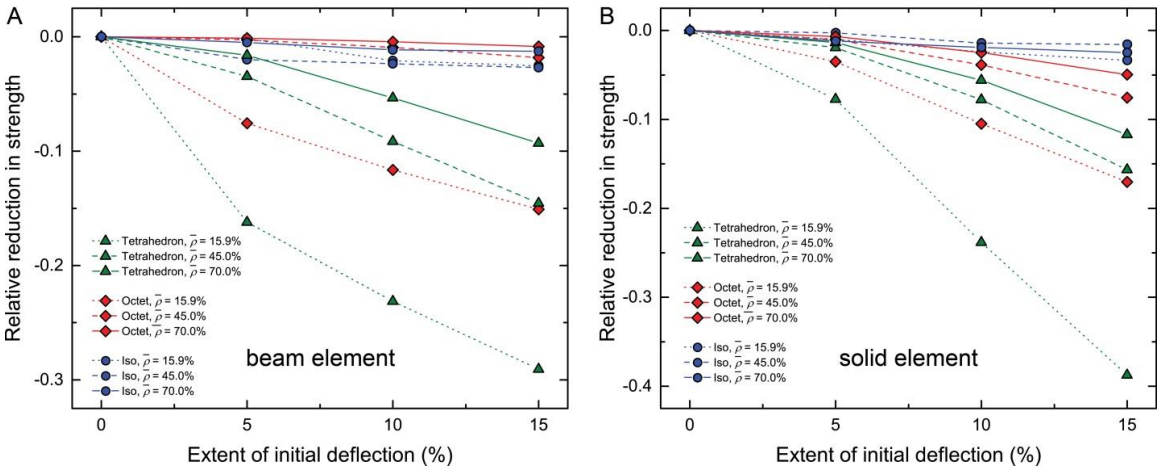

Fig. S5. Relative reduction in strength of nanolattices as a function of the extent of initial deflection. (*A*, *B*) Results from finite element modelling based on beam and solid elements.

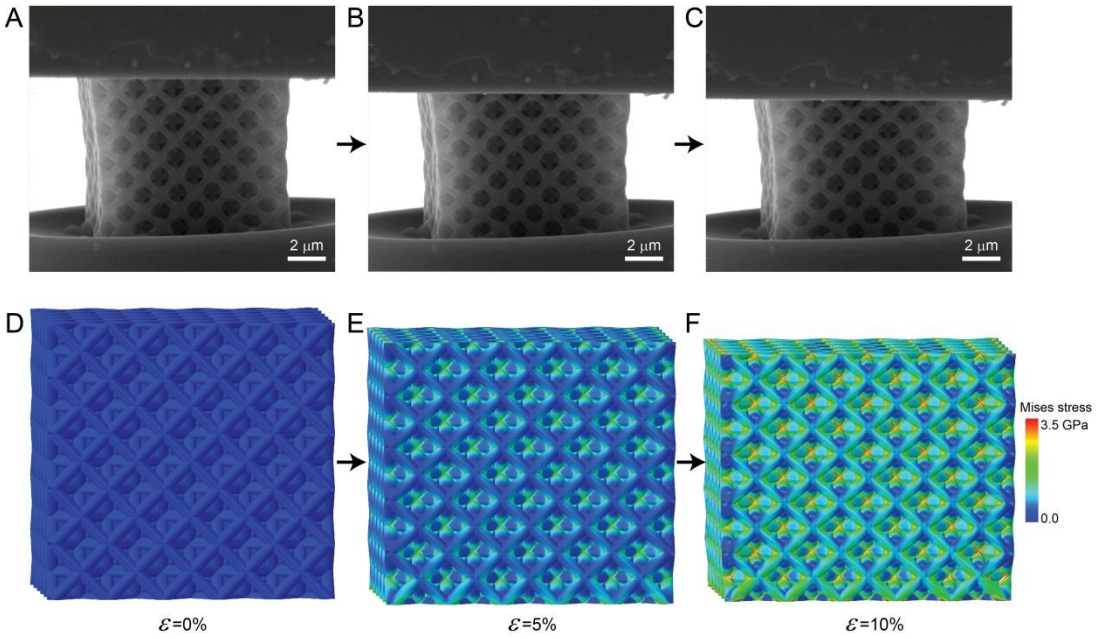

Fig. S6. Comparisons of deformation snapshots in octet-truss nanolattice with relative density of 37.5% from finite element modelling and in-situ experiments. (*A*, *B*, *C*) SEM images from in-situ testing at different strains. (*D*, *E*, *F*) Snapshots from finite element modelling with solid elements at different strains.

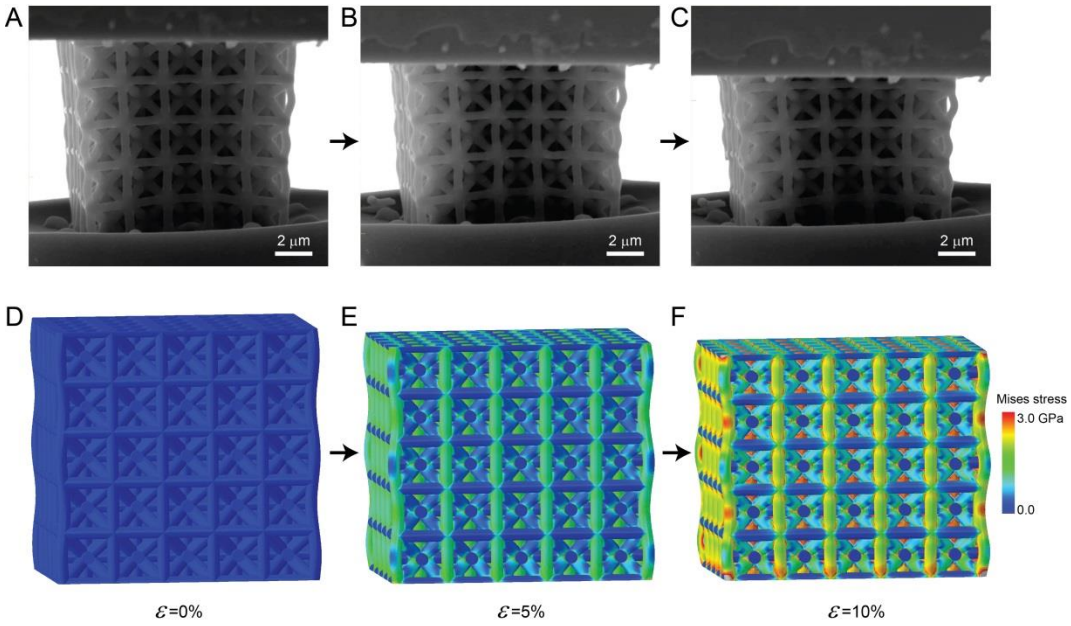

Fig. S7. Comparison of deformation snapshots in an iso-truss nanolattice with relative density of 39.4% from finite element modelling and in-situ experiments. (*A*, *B*, *C*) SEM images from in-situ testing at different strains. (*D*, *E*, *F*) Snapshots from finite element modelling with solid elements at different strains.

Table S1. Mechanical properties of polymer microlattices under compression

Unit cell geometry	Relative density $\bar{\rho}$ (%)	Young's modulus E (MPa)	Strength σ_y (MPa)
Iso	9.21	112	4.47
	12.38	172	7.20
Octet	11.85	89	5.52
	16.22	109	7.49

Movie S1. In-situ uniaxial compression of octet-truss nanolattice with relative density of 37.5%. The nanolattice first underwent the elastic deformation, and then failed due to the brittle fracture. The fracture strength is up to about 300 MPa.

Movie S2. In-situ uniaxial compression of iso-truss nanolattice with relative density of 39.4%. The nanolattice first underwent the elastic deformation, and then failed due to the brittle fracture. The fracture strength is as high as 400 MPa.